

Light-Switchable and Self-Healable Polymer Electrolytes Based on Dynamic Diarylethene and Metal-Ion Coordination

Hui Nie,[§] Nicole S. Schauer,[§] Jeffrey L. Self, Tarnuma Tabassum, Saejin Oh, Zhishuai Geng, Seamus D. Jones, Manuel S. Zayas, Veronica G. Reynolds, Michael L. Chabiny, Craig J. Hawker, Songi Han, Christopher M. Bates, Rachel A. Segalman,^{*} and Javier Read de Alaniz^{*}



Cite This: *J. Am. Chem. Soc.* 2021, 143, 1562–1569



Read Online

ACCESS |



Metrics & More

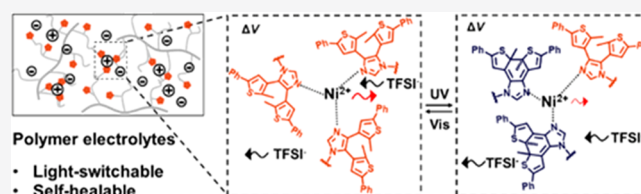


Article Recommendations



Supporting Information

ABSTRACT: Self-healing polymer electrolytes are reported with light-switchable conductivity based on dynamic *N*-donor ligand-containing diarylethene (DAE) and multivalent Ni²⁺ metal-ion coordination. Specifically, a polystyrene polymer grafted with poly(ethylene glycol-*r*-DAE)acrylate copolymer side chains was effectively cross-linked with nickel(II) bis-(trifluoromethanesulfonimide) (Ni(TFSI)₂) salts to form a dynamic network capable of self-healing with fast exchange kinetics under mild conditions. Furthermore, as a photoswitching compound, the DAE undergoes a reversible structural and electronic rearrangement that changes the binding strength of the DAE–Ni²⁺ complex under irradiation. This can be observed in the DAE-containing polymer electrolyte where irradiation with UV light triggers an increase in the resistance of solid films, which can be recovered with subsequent visible light irradiation. The increase in resistance under UV light irradiation indicates a decrease in ion mobility after photoswitching, which is consistent with the stronger binding strength of ring-closed DAE isomers with Ni²⁺. ¹H–¹⁵N heteronuclear multiple-bond correlation nuclear magnetic resonance (HMBC NMR) spectroscopy, continuous wave electron paramagnetic resonance (cw EPR) spectroscopy, and density functional theory (DFT) calculations confirm the increase in binding strength between ring-closed DAE with metals. Rheological and in situ ion conductivity measurements show that these polymer electrolytes efficiently heal to recover their mechanical properties and ion conductivity after damage, illustrating potential applications in smart electronics.



INTRODUCTION

The ability to remotely modulate ion and/or charge transport using light not only is essential for neurological activity in nature¹ but also enables the fabrication of multifunctional smart materials including photoswitchable organic light-emitting transistors,² supramolecular hydrogels,³ metal organic frameworks,⁴ and semiconductors.⁵ By introducing light-responsive functional groups into these materials, the optical and/or electrical properties can be noninvasively tuned with excellent spatial and temporal resolution, making them pivotal components for emerging optoelectronics applications such as smart displays, photodetectors, and logic circuits.^{3,6–8} Among these materials, polymer electrolytes are an attractive platform due to their high ionic conductivity, tunable polymeric scaffold, and robust mechanical properties.^{9,10} Importantly, ion mobility and conductivity in these materials are highly dependent on different types of weak interactions, such as cation–anion,¹¹ polymer–ion,¹² and Lewis acid–base interactions.^{13,14} The rational and noninvasive modulation of these weak interactions by integrating light-responsive moieties into the structure of polymer electrolytes provides an elegant way to tune the ion mobility and conductivity in situ.^{15,16} Huang and co-workers reported supramolecular ion-conducting hydrogels using

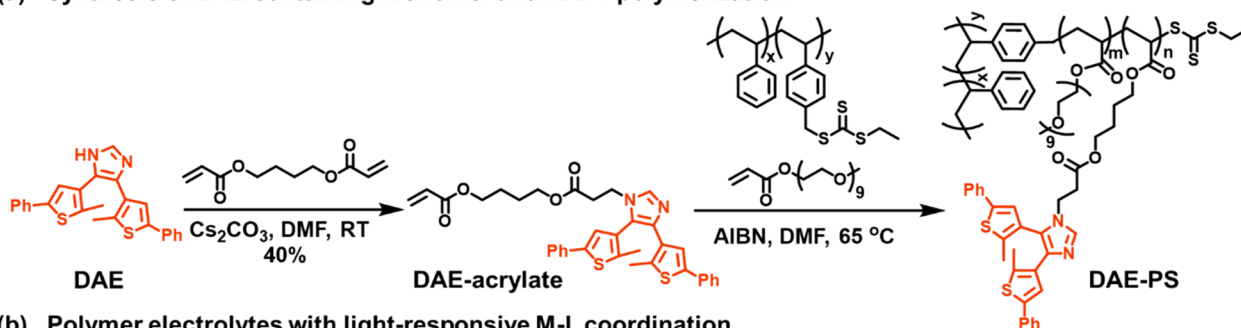
azobenzene to mediate reversible changes in conductivity by competitive guest–host interactions.^{3,17,18} We recently developed a photoswitchable polymeric ionic liquid based on imidazolium-containing diarylethene (DAE) cations and observed that ionic conductivity can be reversibly modulated by tuning the positive charge distribution and cation–anion interaction upon light irradiation.¹⁹ However, current light-responsive ion-conducting polymer electrolytes have relatively poor solid-like mechanical properties, because they are either viscous liquids with a low glass-transition temperature ($T_g \ll 20$ °C) or solvent-containing hydrogels.^{3,19} Consequently, the materials are difficult to integrate into devices.^{20–23} The development of light-responsive, ion-conducting polymers that are mechanically robust, capable of self-healing, and inherently tunable remains a major challenge.

Received: November 12, 2020

Published: January 13, 2021



(a) Synthesis of DAE containing monomer and RAFT polymerization



(b) Polymer electrolytes with light-responsive M-L coordination

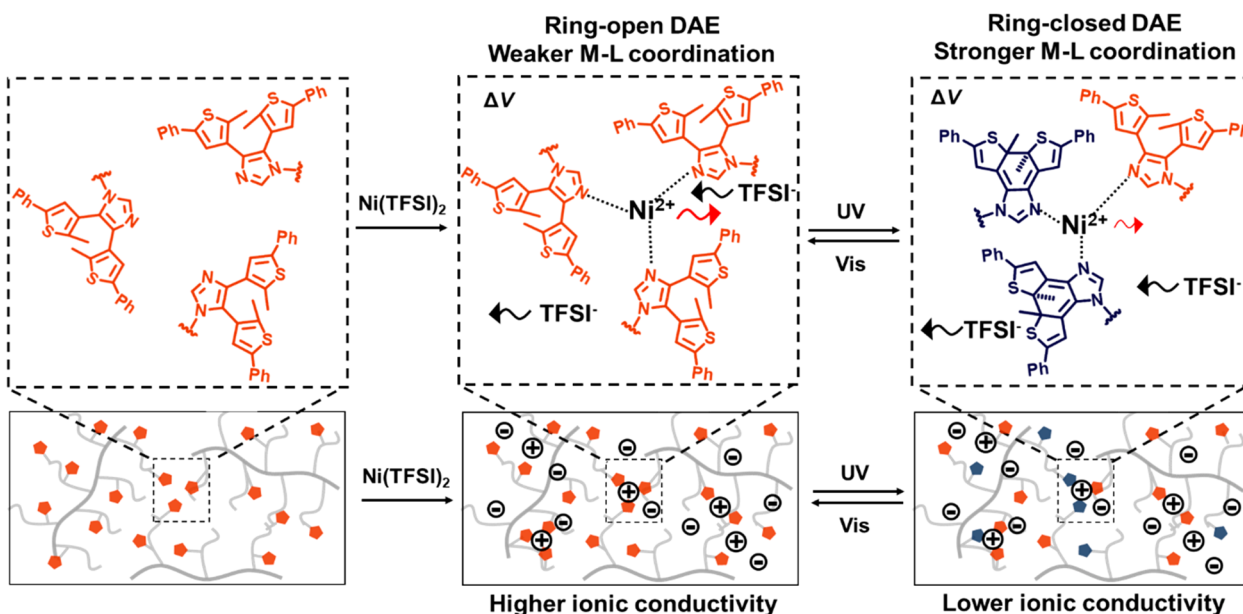


Figure 1. (a) Synthesis of DAE–acrylate monomer and copolymer brushes of DAE–acrylate and PEG–acrylate using RAFT controlled radical polymerization from a PS macro-CTA. (b) Molecular structure and schematic of the polymer network before and after metal salt addition, illustrating salt solvation and formation of DAE–Ni²⁺ complexes. Isomerization of DAE from the ring-open to ring-closed form with UV light irradiation leads to stronger M–L interactions. Reversion back to the ring-open form occurs with visible light irradiation. This reversibly tunable M–L coordination and photostationary state impacts the mobility of metal ions (ionic conductivity).

Here, we demonstrate that cross-linked polymer electrolytes with covalently bonded imidazole-containing DAE ligands and the multivalent metal salt nickel(II) bis-(trifluoromethanesulfonimide) (Ni(TFSI)₂) leads to robust networks that self-heal and reversibly change ionic conductivity in response to light irradiation (Figure 1). Through the stronger binding strength of the metal–ligand (M–L) complex, decreased mobility of Ni²⁺ and thus ionic conductivity are observed in the solid state. This design strategy demonstrates that reversible light-switching and self-healing polymer electrolytes can be engineered with a useful balance of different properties.

RESULTS AND DISCUSSION

Polymer Electrolytes Design and Synthesis. To achieve cross-linked polymer electrolytes with light-controllable ionic conductivity and self-healing properties, a polystyrene (PS) polymer grafted with poly(ethylene glycol-*r*-DAE)acrylate copolymer side chains (DAE–PS) was employed. Inclusion of the PS component enhances the mechanical properties²⁴ of the material, whereas the polyethylene glycol (PEG) monomers are beneficial for ion solvation, and the DAE-containing monomers are used as

light-responsive cross-linking sites. For the synthesis of DAE–PS, the DAE-containing acrylate monomer (DAE–acrylate) was initially prepared via Michael addition of DAE to 1,4-butanediol diacrylate (Figure 1a). The grafted copolymer was then obtained by reversible addition–fragmentation chain transfer polymerization (RAFT) of DAE–acrylate and PEG–acrylate (*M*_n = 480 g/mol) using a previously reported PS macro-chain transfer agent (macro-CTA).²⁴ The macro-CTA used here contains ~140 repeating units of PS with ~10 mol % of the RAFT chain transfer groups along the backbone. After polymerization in DMF, the average degree of polymerization of the randomly grafted copolymer side chains was ~36 repeating units with about 30 mol % DAE as measured by ¹H NMR (Figure S1). According to the literature, a high incorporation of imidazole-containing monomer is essential for efficient cross-linking with metal ions in the materials.²⁴ A linear copolymer of DAE–acrylate (30 mol %) and PEG–acrylate (L-DP) was also synthesized for comparison (Figure S2).

With the DAE–PS brush copolymer architecture in hand, Ni(TFSI)₂ was chosen as a cross-linker (DAE–PS–Ni) based on M–L coordination for the following reasons: (1) from our previous work, the plateau modulus increases by an order of

magnitude after adding $\text{Ni}(\text{TFSI})_2$,²⁵ and (2) metal salts with a TFSI anion feature good solubility and thermal stability.²⁶ A molar ratio $r = 0.1$ ($[\text{Ni}^{2+}]:[\text{DAE-acrylate monomer}]$) was used to balance efficient cross-linking, efficient photoswitching, and ionic conductivity. Incorporation of Ni salt resulted in a change of mechanical properties from a viscous polymer melt to a soft solid, suggesting the formation of Ni-mediated crosslinks between polymer chains. Moreover, as shown in Figure S3, after the addition of $\text{Ni}(\text{TFSI})_2$, the intense absorption band at ca. 276 nm corresponding to π -to- π^* and n-to- π^* transitions of the imidazole and thiophene moieties present in DAE broadens and an absorption shoulder at ca. 290 nm appears. This red-shifted absorption agrees with other metal-imidazole- or pyridine-containing ligand coordination systems and suggests metal-ion binding to the DAE ligands.^{27,28} The DSC traces of DAE-PS with and without $\text{Ni}(\text{TFSI})_2$ show transitions at around -29 and 91 °C (Figure S4), which are assigned as the T_g values of the poly(PEG-DAE) and PS domain,²⁹ respectively. While permanently cross-linked polymer networks are difficult to postprocess,^{30,31} the DAE-PS-Ni network is readily dissolvable and can be reshaped or spin coated on a variety of surfaces.

Photoswitching Properties. Encouraged by these initial results, we next investigated the photochemical behavior of DAE-PS-Ni thin films, which is a driver for many applications of polymer electrolytes.³² Figure 2a depicts representative UV-vis absorption spectra of spin-coated DAE-PS-Ni thin films. Irradiation with UV light (300 nm,

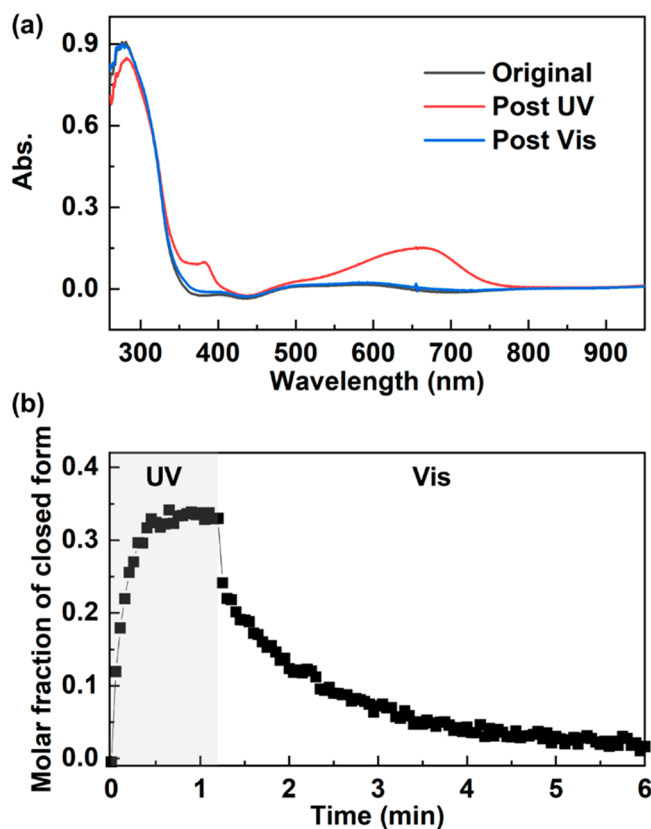


Figure 2. (a) UV-vis absorption spectra of DAE-PS-Ni polymer thin films on ITO before and after UV (300 nm) and broad-band white light irradiation. (b) Kinetic traces of a DAE-PS-Ni polymer ($r = 0.1$) thin film during initial exposure to 300 nm light followed by broad-band white light.

0.6 mW/cm², ~1 min) resulted in a distinct color change from near colorless to blue due to the photocyclization of DAE units. In agreement with the behavior in solution,²⁸ the UV-vis spectra of DAE-PS-Ni films exhibited an absorption at about 276 nm with rapid switching observed upon UV irradiation, leading to the appearance of new band at 660 nm with a shoulder at ~370 nm. These absorption characteristics of ring-open and ring-closed isomers are in accordance with the UV-vis spectra derived from density functional theory (DFT) calculation (Figures S5 and S6). Significantly, subsequent irradiation with visible light (white light, 47 mW/cm², ~6 min) reversed these spectral changes, resulting in color loss, clearly demonstrating the reversible photoswitching nature of supported DAE units in these graft copolymer thin films. In addition, the calculated energy difference between the ring-open and the ring-closed isomers of imidazole-containing DAE is 28.4 kcal/mol, which is similar to reported dithienylbenzene as well as the charged imidazolium-containing DAE from our previous work (Figure S7).³³ To estimate the photostationary state (PSS) of these DAE units, a small molecule model system, butyl acrylate-DAE, was synthesized for easy quantification of PSS in solution by UV-vis spectroscopy and ¹H NMR. The extinction coefficients of ring-open and ring-closed isomers (ϵ_{open} and ϵ_{closed}) were calculated to be ~31 800 (276 nm) and ~37 500 (660 nm) L mol⁻¹ cm⁻¹, respectively (Figures S8–S10). On the basis of the assumption that the model molecule in solution and polymer-supported DAE units in thin films have similar ϵ_{open} and ϵ_{closed} , the PSS of DAE-PS and DAE-PS-Ni thin films is estimated to contain 54 and 34 mol % of the ring-closed isomer (Figures 2b and S10–S12). We also note that the addition of $\text{Ni}(\text{TFSI})_2$ decreased the molar ratio of ring-closed isomers at the PSS in the polymer, possibly due to stabilization of the aromatic imidazole in the ring-open state by the transition metal.³⁴ The thermal relaxation process of this T-type DAE in thin films is shown in Figure S13.

Light-Responsive M-L Coordination. The binding affinity of Ni^{2+} to DAE units in the polymer can be reversibly modulated using different wavelengths of light. When the DAE unit is present as the ring-open isomer, the imidazole ring is aromatic with $(4n + 2)$ p electrons (Figure S14) and the Ni^{2+} ions coordinate with the pyridine-like nitrogen in the ring.^{35,36} Irradiation with UV light triggers cyclization to give the ring-closed isomer with associated electronic rearrangement, leading to a nonaromatic Schiff base. The lone pair of electrons on the Schiff base nitrogen also has the ability to coordinate with a Ni^{2+} cation,³⁷ and the higher electron density of the nitrogen atom increases the σ -donor strength for M-L coordination.³⁵ As shown with ¹H-¹⁵N heteronuclear multiple bond correlation (HMBC) NMR spectra of a model DAE molecule (methyl DAE), the pyridine-like nitrogen experiences an upfield chemical shift from 260.9 to 235.8 ppm upon UV light irradiation (300 nm, 1.3 mW/cm², 20 min in an NMR tube). This indicates that the nitrogen atoms in the ring-closed isomer feature higher electron density than the ring-open isomer (Figures 3a and S15). Here, an ¹⁵N NMR spectrum of ¹⁵N-labeled methyl DAE allowed the peaks of each nitrogen atom in the structure to be fully assigned (Figure S16). On the basis of these NMR results, the ring-closed isomer has stronger σ bonding with the metal ions. Continuous wave electron paramagnetic resonance spectroscopy (cw EPR) was then used to further assess the strength of M-L coordination in these polymer electrolytes before and after isomerization. Cu^{2+} was

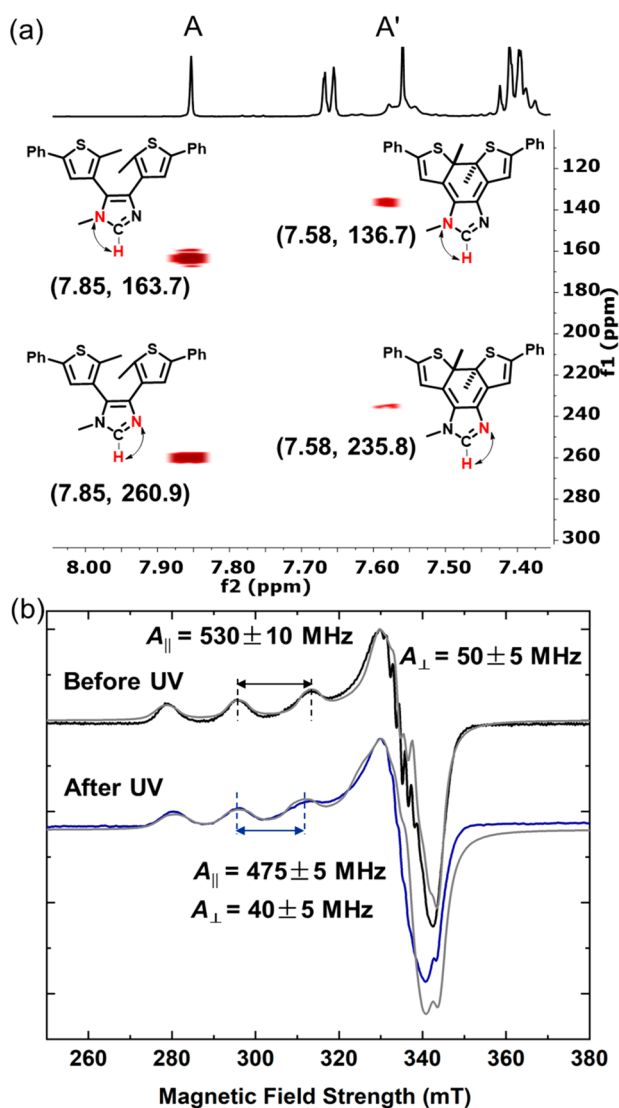


Figure 3. (a) ^1H – ^{15}N HMBC NMR spectra of methyl DAE after UV light (300 nm) irradiation. Fraction of the ring-open isomers was switched to ring-closed isomers upon UV irradiation. (b) Continuous wave EPR signals of DAE–PS Cu(TFSI) $_2$ ($r = 0.1$) in DCM with $[\text{Cu}^{2+}] = 5$ mM before and after UV (300 nm) light irradiation.

selected as a local probe to detect the changing environment around metal ions while photoswitching DAE for the following reasons. First, Cu^{2+} has one unpaired electron in its d^9 orbital and two magnetically active and naturally occurring isotopes (^{63}Cu 69.13%; ^{65}Cu 30.83%) with nuclear spin $I = 3/2$, resulting in hyperfine interactions between the electron and the nuclear spins to be studied. Second, the resulting strong spin–orbit coupling and electron–ligand field interactions lead to anisotropy of the g value and hyperfine (A) value, which are especially sensitive to the local environment around Cu^{2+} . 38 Third, Cu^{2+} –imidazole EPR spectra are well studied in the literature, which provides a basis for analysis of the Cu^{2+} –DAE systems studied in this work. 39 Fourth, the DAE units undergo reversible photoswitching in the presence of Cu^{2+} (Figure S17), which is similar to Ni^{2+} . A solution sample of DAE–PS polymer with $\text{Cu}(\text{TFSI})_2$ ($[\text{Cu}^{2+}] = 5$ mM, molar ratio Cu^{2+} :DAE = 0.1) in DCM was used for EPR measurements, and as shown in Figure 3b, the EPR spectra of polymer and $\text{Cu}(\text{TFSI})_2$ resemble typical Cu^{2+} –imidazole systems. 40 The

A_{\parallel} and A_{\perp} values of DAE–PS– $\text{Cu}(\text{TFSI})_2$ before UV irradiation are 530 ± 10 and 50 ± 5 MHz, and g_{\parallel} and g_{\perp} values are 2.045 ± 0.001 and 2.260 ± 0.005 , respectively, as obtained from simulation (using the “pepper” function for solid-state cw spectra in EasySpin, a MATLAB toolbox). These values are similar to those reported for other Cu^{2+} –imidazole systems. 41 In addition, a value of $g_{\parallel} < 2.3$ implies covalent character for the Cu^{2+} –DAE coordination. 42 After being subjected to UV irradiation, the percentage of ring-closed isomers in DAE–PS– $\text{Cu}(\text{TFSI})_2$ solution increased as evidenced by pump–probe measurement (Figure S17) with concomitant EPR spectral changes being observed. Compared with the sample before UV light irradiation, the g value does not change but A_{\parallel} (475 ± 5 MHz) and A_{\perp} (40 ± 5 MHz) decrease. The value of α , calculated from a model developed by Kivelson and co-workers, is used to quantify the covalency of $\text{DAE}-\text{Cu}^{2+}$ coordination before and after UV light irradiation 43

$$\alpha^2 = -\left(\frac{A_{\parallel}}{P}\right) + (g_{\parallel} - g_e) + \frac{3}{7}(g_{\perp} - g_e) + 0.04$$

where P is the interaction dipolar term of the free Cu^{2+} ion (0.036 cm^{-1}) and g_e is the g factor of a free electron (2.0023). For a completely ionic bond $\alpha^2 = 1$, whereas for a completely covalent bond $\alpha^2 = 0.5$. We find that the α^2 values decrease from 0.68 to 0.63 after UV irradiation, suggesting the Cu^{2+} –DAE coordination increases in covalency. Another noteworthy observation is the broadening of spectra and superhyperfine features arising from ^{14}N coupling after UV irradiation. This is consistent with an increased covalency of Cu^{2+} – ^{14}N bonds that can result in concurrently stronger hyperfine coupling interactions with the hydrogen atoms in the DAE ring, yielding an increase in the number of EPR lines and less well-resolved features in the ^{14}N region. 44 In addition to the NMR and EPR observations, DFT calculations corroborate the decreased N– Ni^{2+} bond lengths of ring-open and ring-closed DAE isomers (Table S1). The presence of Ni^{2+} lowers the DFT-calculated difference in energy between the ring-open and the ring-closed isomers to ~ 13 kcal/mol. This difference can be attributed to the higher binding energy of the ring-closed isomer to Ni^{2+} (Figure S18). In summary, the combination of ^1H – ^{15}N HMBC NMR, EPR spectral analysis, and DFT calculations indicates that the ring-closed isomer has a stronger interaction with metal ions than the ring-open isomer.

Light-Switchable Ionic Conductivity. The exciting ability to reversibly switch the M–L coordination strength with light holds potential for tuning ionic conductivity with external stimuli. The bulk ionic conductivity of DAE–PS–Ni with $r = 0.1$ salt loading is around 3.9×10^{-7} S/cm at room temperature (Figure 4a) with an activation energy of 0.61 eV from the Arrhenius equation, which are within the typical range of PEO-based polymer electrolytes. 45 It is worth noting that the ionic conductivity included both Ni^{2+} and TFSI^- ions transport, similar to our previous study. 25,38,46 The light-switchable DAE ligand modulates the mobility of Ni^{2+} and thus the ionic conductivity. From X-ray scattering, no obvious features of aggregation or crystallization of added ions were observed, suggesting that ions are homogeneously dispersed in the material (Figure S19). To monitor the change of ionic conductivity with light irradiation, in situ through-plane analysis of spin-coated DAE–PS–Ni thin films was carried out on pre-cleaned ITO with evaporated Au electrodes as top

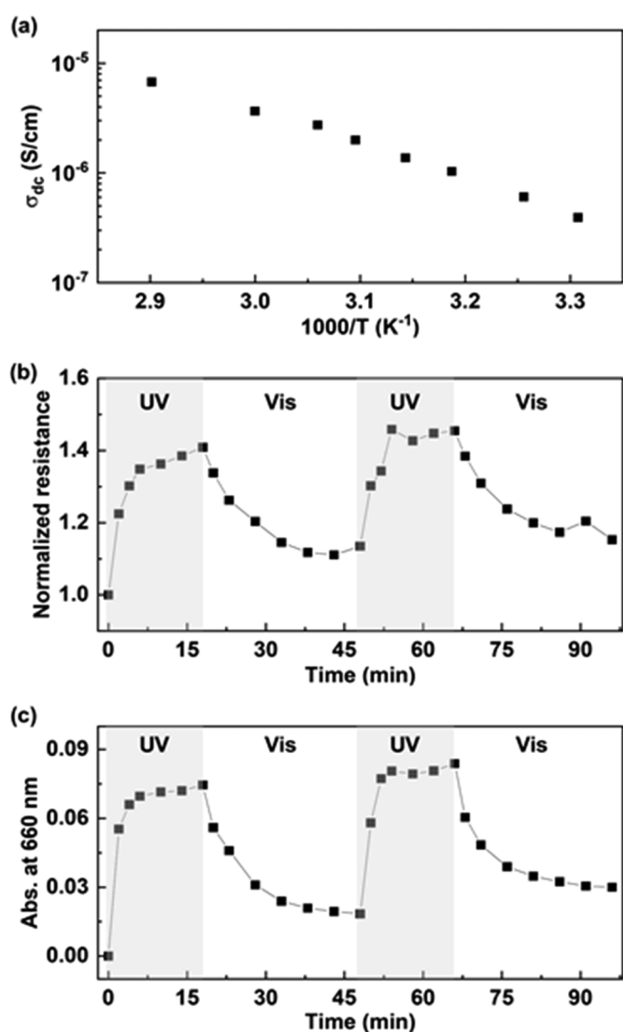


Figure 4. (a) Temperature dependence of the ionic conductivity for a bulk DAE-PS-Ni with $r = 0.1$ before photoswitching. (b) Normalized resistance of DAE-PS-Ni thin films under UV (300 nm) and white light irradiation. (c) Variation of the absorption intensity of ring-closed isomers in DAE-PS-Ni thin films at 660 nm with UV (300 nm) and white light irradiation.

contacts (Figure S20).¹⁹ As shown in Figure 4b, the resistance of the polymer thin film increased upon UV irradiation (313 nm, 0.8 mW/cm², different time intervals) and subsequently decreased upon exposure to visible light (white light, 0.4 mW/cm², different time intervals). These trends are consistent with the NMR and EPR results, which indicate that polymers with ring-closed DAE units have stronger M-L coordination and thus decreased Ni²⁺ ion mobility (higher resistance) than the corresponding ring-open isomers. To further support that resistance changes of DAE-PS-Ni are induced by the photoswitching of DAE, the absorption intensity of the ring-closed isomer was monitored with the same light irradiation conditions as during conductivity measurements. As shown in Figure 4c, the kinetics and time scale of ring-open to ring-closed isomerization are in quantitative agreement with the resistance variation. Significantly, the ability to tune conductivity with light irradiation was reproducible for at least 6 cycles (Figure S21), albeit with a slight variation of resistance possibly due to minor degradation of the DAE units.⁴⁷ The spatial control of photochemical regulation further enables the patterning of local conductivity in polymer thin films using UV light (Figure S22).

Self-Healing Properties. In addition to light-induced changes in conductivity, the DAE-PS-Ni polymer electrolytes are soft solids that can self-heal under mild conditions. As shown in Figure 5a, the storage modulus (G') of DAE-PS-Ni is higher than the loss modulus (G'') across 0.01–10 Hz as measured by oscillatory rheology at room temperature. These solid-like properties arise at fast and intermediate time scales due to the transient M-L cross-links with a frequency dependence that matches the molecular exchange dynamics.^{24,48} In contrast, samples synthesized with no PS component or without Ni(TFSI)₂ are viscous liquids at all frequencies (Figure S23). These results suggest that the synergistic combination of a PS component and DAE-Ni²⁺ coordination is required to generate a soft solid as M-L bonds are too labile at room temperature. Since dynamic DAE-Ni²⁺ complexes reside in the percolating PEG domain, DAE-PS-Ni polymer electrolytes can self-heal. As demonstrated in Figures 5a and S24, a DAE-PS-Ni sample that was damaged subsequently recovered its original properties after heating on the rheometer plate at 45 °C under nitrogen for 1.5 h. Figures

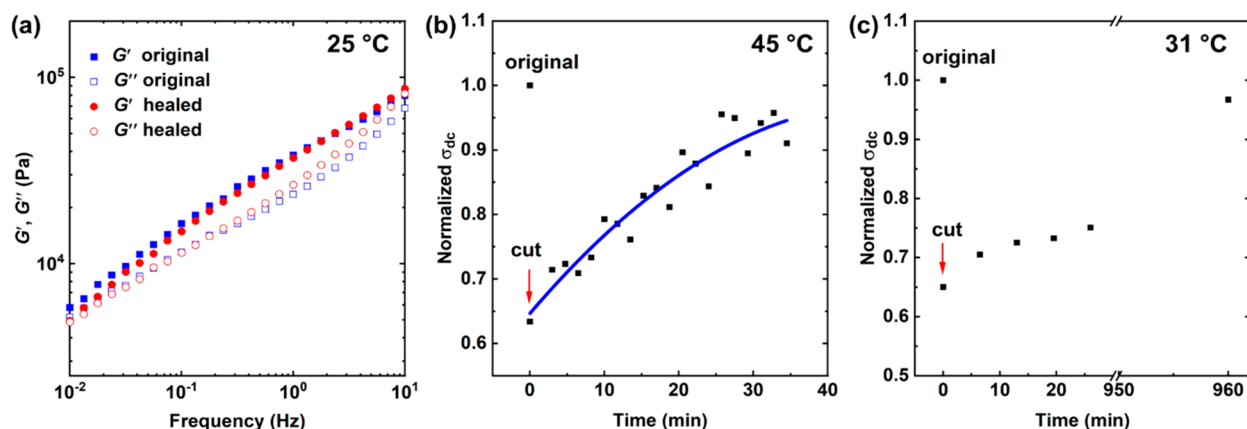


Figure 5. (a) Room-temperature frequency sweeps of original and healed (45 °C, 1.5 h) polymer electrolyte. (b) Normalized ionic conductivity before and after the polymer electrolyte was cut with a blade, showing 93% recovery of the initial conductivity after 35 min at 45 °C. (c) Normalized ionic conductivity before and after the polymer electrolyte was cut with a blade (~50% of the film thickness) and 96% of the initial conductivity was recovered after 16 h at room temperature (31 °C).

Sb and Sc show that the ionic conductivity of DAE-PS-Ni is significantly reduced after applying a deep cut (~50% of the film thickness). Notably, 94% and 96% of the ionic conductivity is restored after 35 min at 45 °C and 16 h at room temperature, respectively. Importantly, healed samples also show similar ionic conductivity when drop cast (~550 μm thickness) on a quartz slide with Au electrodes deposited on the top surface (Figures S25 and S26). The time required for healing at 45 °C is shorter than that at room temperature, which we believe originates from faster metal-ion exchange kinetics and a decrease in the modulus (G' , G'') as the temperature of the material increases (Figures S27 and S28). The accelerated polymer dynamics at increased temperature results in faster self-healing behavior which is consistent with literature reports.^{49,50} The efficient recovery of not only the mechanical properties but also the electronic properties showcases the advantage of a self-healing M-L coordination network.

CONCLUSION

Incorporation of photoswitchable units into polymer electrolytes constitutes a design strategy for functional materials with remotely tunable conductivity. On the basis of DAE as a photoresponsive building block, the reversible electronic rearrangement between ring-open and ring-closed states changes the binding strength of ligands to multivalent metal ions. With the appropriate choice of polymeric building blocks, these materials are soft solids at room temperature that can self-heal under mild heating and change ionic conductivity in response to light irradiation. Our results demonstrate that light-responsive M-L coordination is a versatile design concept to create novel polymer electrolytes with potential applications ranging from photodetectors to smart circuits and soft robotics.

ASSOCIATED CONTENT

Supporting Information

The Supporting Information is available free of charge at <https://pubs.acs.org/doi/10.1021/jacs.0c11894>.

General methods, synthesis and characterization of materials, photoisomerization studies, DFT calculations, ion conductivity measurements, self-healing studies (PDF)

AUTHOR INFORMATION

Corresponding Authors

Rachel A. Segalman – Materials Department, Materials Research Laboratory, and Department of Chemical Engineering, University of California–Santa Barbara, Santa Barbara, California 93106, United States; orcid.org/0000-0002-4292-5103; Email: segalman@engineering.ucsb.edu

Javier Read de Alaniz – Department of Chemistry and Biochemistry, University of California–Santa Barbara, Santa Barbara, California 93106, United States; orcid.org/0000-0003-2770-9477; Email: javier@chem.ucsb.edu

Authors

Hui Nie – Department of Chemistry and Biochemistry, University of California–Santa Barbara, Santa Barbara, California 93106, United States

Nicole S. Schauer – Materials Department and Materials Research Laboratory, University of California–Santa Barbara, Santa Barbara, California 93106, United States

Jeffrey L. Self – Department of Chemistry and Biochemistry, University of California–Santa Barbara, Santa Barbara, California 93106, United States

Tarnuma Tabassum – Department of Chemistry and Biochemistry, University of California–Santa Barbara, Santa Barbara, California 93106, United States

Saejin Oh – Department of Chemistry and Biochemistry, University of California–Santa Barbara, Santa Barbara, California 93106, United States

Zhishuai Geng – Materials Department and Materials Research Laboratory, University of California–Santa Barbara, Santa Barbara, California 93106, United States

Seamus D. Jones – Department of Chemical Engineering and Materials Research Laboratory, University of California–Santa Barbara, Santa Barbara, California 93106, United States

Manuel S. Zayas – Department of Chemistry and Biochemistry, University of California–Santa Barbara, Santa Barbara, California 93106, United States

Veronica G. Reynolds – Materials Department and Materials Research Laboratory, University of California–Santa Barbara, Santa Barbara, California 93106, United States

Michael L. Chabinye – Materials Department and Materials Research Laboratory, University of California–Santa Barbara, Santa Barbara, California 93106, United States;

orcid.org/0000-0003-4641-3508

Craig J. Hawker – Department of Chemistry and Biochemistry, University of California–Santa Barbara, Santa Barbara, California 93106, United States; Materials Department and Materials Research Laboratory, University of California–Santa Barbara, Santa Barbara, California 93106, United States; orcid.org/0000-0001-9951-851X

Songi Han – Department of Chemistry and Biochemistry, University of California–Santa Barbara, Santa Barbara, California 93106, United States; Department of Chemical Engineering, University of California–Santa Barbara, Santa Barbara, California 93106, United States; orcid.org/0000-0001-6489-6246

Christopher M. Bates – Department of Chemistry and Biochemistry, University of California–Santa Barbara, Santa Barbara, California 93106, United States; Materials Department and Materials Research Laboratory, University of California–Santa Barbara, Santa Barbara, California 93106, United States; orcid.org/0000-0002-1598-794X

Complete contact information is available at: <https://pubs.acs.org/doi/10.1021/jacs.0c11894>

Author Contributions

[§]H.N. and N.S.S.: These authors contributed equally.

Funding

This work was supported by the MRSEC Program of the National Science Foundation under Award No. DMR 1720256 (IRG-2). The research reported here made use of shared facilities of the National Science Foundation (NSF) Materials Research Science and Engineering Center at UC Santa Barbara, DMR-1720256. The UCSB MRSEC is a member of the Materials Research Facilities Network (www.mrfn.org). N.S.S gratefully acknowledges the Fannie and John Hertz Foundation and the National Science Foundation Graduate

Research Fellowship Program under Grant 1650114. V.G.R. gratefully acknowledges the National Science Foundation Graduate Research Fellowship Program under Grant 1650114. Use was made of computational facilities purchased with funds from the National Science Foundation (CNS-1725797) and administered by the Center for Scientific Computing (CSC). The CSC is supported by the California NanoSystems Institute and the Materials Research Science and Engineering Center (MRSEC; NSF DMR 1720256) at UC Santa Barbara. Any opinions, findings, and conclusions or recommendations expressed in this material are those of the authors and do not necessarily reflect the views of the National Science Foundation. This work was supported in part by NSF Major Research Instrumentation award, MRI-1920299, for magnetic resonance instrumentation. X-ray scattering measurements were performed at the National Synchrotron Light Source II (NSLS-II, beamline 11-BM, Brookhaven National Laboratory).

Notes

The authors declare no competing financial interest.

REFERENCES

- (1) Beck, S.; Yu-Strzelczyk, J.; Pauls, D.; Constantin, O. M.; Gee, C. E.; Ehmman, N.; Kittel, R. J.; Nagel, G.; Gao, S. Synthetic Light-Activated Ion Channels for Optogenetic Activation and Inhibition. *Front. Neurosci.* **2018**, *12*, 643.
- (2) Hou, L.; Zhang, X.; Cotella, G. F.; Carnicella, G.; Herder, M.; Schmidt, B. M.; Pätzelt, M.; Hecht, S.; Cacialli, F.; Samori, P. Optically Switchable Organic Light-Emitting Transistors. *Nat. Nanotechnol.* **2019**, *14* (4), 347–353.
- (3) Wang, H.; Zhu, C. N.; Zeng, H.; Ji, X.; Xie, T.; Yan, X.; Wu, Z. L.; Huang, F. Reversible Ion-Conducting Switch in a Novel Single-Ion Supramolecular Hydrogel Enabled by Photoresponsive Host–Guest Molecular Recognition. *Adv. Mater.* **2019**, *31* (12), 1807328–1807335.
- (4) Dolgoplova, E. A.; Galitskiy, V. A.; Martin, C. R.; Gregory, H. N.; Yarbrough, B. J.; Rice, A. M.; Berseneva, A. A.; Ejegbavwo, O. A.; Stephenson, K. S.; Kittikhunnatham, P.; Karakalos, S. G.; Smith, M. D.; Greytak, A. B.; Garashchuk, S.; Shustova, N. B. Connecting Wires: Photoinduced Electronic Structure Modulation in Metal–Organic Frameworks. *J. Am. Chem. Soc.* **2019**, *141* (13), 5350–5358.
- (5) Park, S.; Fukuda, K.; Wang, M.; Lee, C.; Yokota, T.; Jin, H.; Jinno, H.; Kimura, H.; Zalar, P.; Matsuhisa, N.; Umezumi, S.; Bazan, G. C.; Someya, T. Ultraflexible Near-Infrared Organic Photodetectors for Conformal Photoplethysmogram Sensors. *Adv. Mater.* **2018**, *30* (34), 1802359–1802366.
- (6) Cai, S.; Xu, X.; Yang, W.; Chen, J.; Fang, X. Materials and Designs for Wearable Photodetectors. *Adv. Mater.* **2019**, *31* (18), 1808138–1808152.
- (7) Leydecker, T.; Herder, M.; Pavlica, E.; Bratina, G.; Hecht, S.; Orgiu, E.; Samori, P. Flexible Non-Volatile Optical Memory Thin-Film Transistor Device with over 256 Distinct Levels Based on an Organic Bicomponent Blend. *Nat. Nanotechnol.* **2016**, *11* (9), 769–775.
- (8) Nie, H.; Self, J. L.; Kuenstler, A. S.; Hayward, R. C.; Read de Alaniz, J. Multiaddressable Photochromic Architectures: From Molecules to Materials. *Adv. Opt. Mater.* **2019**, *7* (16), 1900224–1900245.
- (9) Shi, L.; Zhu, T.; Gao, G.; Zhang, X.; Wei, W.; Liu, W.; Ding, S. Highly Stretchable and Transparent Ionic Conducting Elastomers. *Nat. Commun.* **2018**, *9*, 2630.
- (10) Yin, X. Y.; Zhang, Y.; Cai, X.; Guo, Q.; Yang, J.; Wang, Z. L. 3D Printing of Ionic Conductors for High-Sensitivity Wearable Sensors. *Mater. Horiz.* **2019**, *6* (4), 767–780.
- (11) Ma, Q.; Zhang, H.; Zhou, C.; Zheng, L.; Cheng, P.; Nie, J.; Feng, W.; Hu, Y. S.; Li, H.; Huang, X.; Chen, L.; Armand, M.; Zhou, Z. Single Lithium-Ion Conducting Polymer Electrolytes Based on a Super-Delocalized Polyaniion. *Angew. Chem., Int. Ed.* **2016**, *55* (7), 2521–2525.
- (12) Zhang, H.; Chen, F.; Lakuntza, O.; Oteo, U.; Qiao, L.; Martinez-Ibañez, M.; Zhu, H.; Carrasco, J.; Forsyth, M.; Armand, M. Suppressed Mobility of Negative Charges in Polymer Electrolytes with an Ether-Functionalized Anion. *Angew. Chem.* **2019**, *131* (35), 12198–12203.
- (13) McBreen, J.; Lee, H. S.; Yang, X. Q.; Sun, X. New Approaches to the Design of Polymer and Liquid Electrolytes for Lithium Batteries. *J. Power Sources* **2000**, *89* (2), 163–167.
- (14) Kurono, R.; Mehta, M. A.; Inoue, T.; Fujinami, T. Preparation and Characterization of Lithium Ion Conducting Borosiloxane Polymer Electrolytes. *Electrochim. Acta* **2001**, *47* (3), 483–487.
- (15) Yam, V. W. W.; Lee, J. K. W.; Ko, C. C.; Zhu, N. Photochromic Diarylethene-Containing Ionic Liquids and N-Heterocyclic Carbenes. *J. Am. Chem. Soc.* **2009**, *131* (3), 912–913.
- (16) Sumitani, R.; Mochida, T. Metal-Containing Poly(Ionic Liquid) Exhibiting Photogeneration of Coordination Network: Reversible Control of Viscoelasticity and Ionic Conductivity. *Macromolecules* **2020**, *53* (16), 6968–6974.
- (17) Yan, X.; Xu, D.; Chen, J.; Zhang, M.; Hu, B.; Yu, Y.; Huang, F. A Self-Healing Supramolecular Polymer Gel with Stimuli-Responsiveness Constructed by Crown Ether Based Molecular Recognition. *Polym. Chem.* **2013**, *4* (11), 3312–3322.
- (18) Zhang, M.; Xu, D.; Yan, X.; Chen, J.; Dong, S.; Zheng, B.; Huang, F. Self-Healing Supramolecular Gels Formed by Crown Ether Based Host–Guest Interactions. *Angew. Chem., Int. Ed.* **2012**, *51* (28), 7011–7015.
- (19) Nie, H.; Schausser, N. S.; Dolinski, N. D.; Hu, J.; Hawker, C. J.; Segalman, R. A.; Read de Alaniz, J. Light-Controllable Ionic Conductivity in a Polymeric Ionic Liquid. *Angew. Chem., Int. Ed.* **2020**, *59* (13), 5123–5128.
- (20) Feig, V. R.; Tran, H.; Lee, M.; Bao, Z. Mechanically Tunable Conductive Interpenetrating Network Hydrogels That Mimic the Elastic Moduli of Biological Tissue. *Nat. Commun.* **2018**, *9*, 2740.
- (21) Lopez, J.; Mackanic, D. G.; Cui, Y.; Bao, Z. Designing Polymers for Advanced Battery Chemistries. *Nat. Rev. Mater.* **2019**, *4* (5), 312–330.
- (22) Lee, G. H.; Moon, H.; Kim, H.; Lee, G. H.; Kwon, W.; Yoo, S.; Myung, D.; Yun, S. H.; Bao, Z.; Hahn, S. K. Multifunctional Materials for Implantable and Wearable Photonic Healthcare Devices. *Nat. Rev. Mater.* **2020**, *5* (2), 149–165.
- (23) Lopez, J.; Sun, Y.; Mackanic, D. G.; Lee, M.; Foudeh, A. M.; Song, M. S.; Cui, Y.; Bao, Z. A Dual-Crosslinking Design for Resilient Lithium-Ion Conductors. *Adv. Mater.* **2018**, *30* (43), 1804142–1804150.
- (24) Mozhdzhehi, D.; Ayala, S.; Cromwell, O. R.; Guan, Z. Self-Healing Multiphase Polymers via Dynamic Metal–Ligand Interactions. *J. Am. Chem. Soc.* **2014**, *136* (46), 16128–16131.
- (25) Sanoja, G. E.; Schausser, N. S.; Bartels, J. M.; Evans, C. M.; Helgeson, M. E.; Seshadri, R.; Segalman, R. A. Ion Transport in Dynamic Polymer Networks Based on Metal–Ligand Coordination: Effect of Cross-Linker Concentration. *Macromolecules* **2018**, *51* (5), 2017–2026.
- (26) Huang, M.; Feng, S.; Zhang, W.; Giordano, L.; Chen, M.; Amanchukwu, C. V.; Anandakathir, R.; Shao-Horn, Y.; Johnson, J. A. Fluorinated Aryl Sulfonimide Tagged (FAST) Salts: Modular Synthesis and Structure–Property. *Energy Environ. Sci.* **2018**, *11*, 1326–1334.
- (27) Rao, Y. L.; Chortos, A.; Pfattner, R.; Lissel, F.; Chiu, Y. C.; Feig, V.; Xu, J.; Kurosawa, T.; Gu, X.; Wang, C.; He, M.; Chung, J. W.; Bao, Z. Stretchable Self-Healing Polymeric Dielectrics Cross-Linked through Metal–Ligand Coordination. *J. Am. Chem. Soc.* **2016**, *138* (18), 6020–6027.
- (28) Lee, P. H. M.; Ko, C. C.; Zhu, N.; Yam, V. W. W. Metal Coordination-Assisted near-Infrared Photochromic Behavior: A Large Perturbation on Absorption Wavelength Properties of N,N-Donor Ligands Containing Diarylethene Derivatives by Coordination to the

Rhenium(I) Metal Center. *J. Am. Chem. Soc.* **2007**, *129* (19), 6058–6059.

(29) Rosati, D.; Perrin, M.; Navard, P.; Harabagiu, V.; Pinteala, M.; Simionescu, B. C. Synthesis of Poly(Styrene-Dimethylsiloxane) Block Copolymers: Influence of the Phase-Separated Morphologies on the Thermal Behaviors. *Macromolecules* **1998**, *31* (13), 4301–4308.

(30) Rikkou-Kalourkoti, M.; Patrickios, C. S.; Georgiou, T. K. *Model Networks and Functional Conetworks*; Elsevier B.V., 2012; Vol. 6, pp 293–305.

(31) Elling, B. R.; Dichtel, W. R. Reprocessable Cross-Linked Polymer Networks: Are Associative Exchange Mechanisms Desirable? *ACS Cent. Sci.* **2020**, *6* (9), 1488–1496.

(32) Choudhury, S.; Stalin, S.; Vu, D.; Warren, A.; Deng, Y.; Biswal, P.; Archer, L. A. Solid-State Polymer Electrolytes for High-Performance Lithium Metal Batteries. *Nat. Commun.* **2019**, *10*, 4398.

(33) Oruganti, B.; Pál Kalapos, P.; Bhargav, V.; London, G.; Durbeej, B. Photoinduced Changes in Aromaticity Facilitate Electrocyclization of Dithienylbenzene Switches. *J. Am. Chem. Soc.* **2020**, *142* (32), 13941–13953.

(34) Świdorski, G.; Wilczewska, A. Z.; Świsłocka, R.; Kalinowska, M.; Lewandowski, W. Spectroscopic (IR, Raman, UV–Vis) Study and Thermal Analysis of 3d-Metal Complexes with 4-Imidazolecarboxylic Acid. *J. Therm. Anal. Calorim.* **2018**, *134* (1), 513–525.

(35) Sundberg, R. J.; Martin, R. B. Interactions of Histidine and Other Imidazole Derivatives with Transition Metal Ions in Chemical and Biological Systems. *Chem. Rev.* **1974**, *74* (4), 471–517.

(36) Andersson Trojer, M.; Movahedi, A.; Blanck, H.; Nydén, M. Imidazole and Triazole Coordination Chemistry for Antifouling Coatings. *J. Chem.* **2013**, *2013*, 946739.

(37) Yousif, E.; Majeed, A.; Al-Sammarrae, K.; Salih, N.; Salimon, J.; Abdullah, B. Metal Complexes of Schiff Base: Preparation, Characterization and Antibacterial Activity. *Arabian J. Chem.* **2017**, *10*, S1639–S1644.

(38) Schausser, N. S.; Grzetic, D. J.; Tabassum, T.; Kliegle, G. A.; Le, M. L.; Susca, E. M.; Antoine, S.; Keller, T. J.; Delaney, K. T.; Han, S.; Seshadri, R.; Fredrickson, G. H.; Segalman, R. A. The Role of Backbone Polarity on Aggregation and Conduction of Ions in Polymer Electrolytes. *J. Am. Chem. Soc.* **2020**, *142* (15), 7055–7065.

(39) Ritterskamp, N.; Sharples, K.; Richards, E.; Folli, A.; Chiesa, M.; Platts, J. A.; Murphy, D. M. Understanding the Coordination Modes of [Cu(Acac)₂(Imidazole)_{N = 1,2}] Adducts by EPR, ENDOR, HYSCORE, and DFT Analysis. *Inorg. Chem.* **2017**, *56* (19), 11862–11875.

(40) Bonomo, R. P.; Riggi, F.; Di Bilio, A. J. EPR Reinvestigation of the Copper(II)-Imidazole System. *Inorg. Chem.* **1988**, *27* (14), 2510–2512.

(41) Godlewska, S.; Jezierska, J.; Baranowska, K.; Augustin, E.; Dołęga, A. Copper(II) Complexes with Substituted Imidazole and Chlorido Ligands: X-Ray, UV-Vis, Magnetic and EPR Studies and Chemotherapeutic Potential. *Polyhedron* **2013**, *65*, 288–297.

(42) Andersson, M.; Hedin, J.; Johansson, P.; Nordström, J.; Nydén, M. Coordination of Imidazoles by Cu(II) and Zn(II) as Studied by NMR Relaxometry, EPR, Far-FTIR Vibrational Spectroscopy and Ab Initio Calculations: Effect of Methyl Substitution. *J. Phys. Chem. A* **2010**, *114* (50), 13146–13153.

(43) Kivelson, D.; Neiman, R. ESR Studies on the Bonding in Copper Complexes. *J. Chem. Phys.* **1961**, *35* (1), 149–155.

(44) Nonaka, Y.; Tokii, T.; Kida, S. Factors Affecting the Line-Width of Nitrogen Superhyperfine Structure in the ESR Spectra of Copper(II) Complexes. *Bull. Chem. Soc. Jpn.* **1974**, *47* (2), 312–315.

(45) Polu, A. R.; Rhee, H. W. Ionic Liquid Doped PEO-Based Solid Polymer Electrolytes for Lithium-Ion Polymer Batteries. *Int. J. Hydrogen Energy* **2017**, *42* (10), 7212–7219.

(46) Schausser, N. S.; Sanoja, G. E.; Bartels, J. M.; Jain, S. K.; Hu, J. G.; Han, S.; Walker, L. M.; Helgeson, M. E.; Seshadri, R.; Segalman, R. A. Decoupling Bulk Mechanics and Mono- and Multivalent Ion Transport in Polymers Based on Metal-Ligand Coordination. *Chem. Mater.* **2018**, *30* (16), 5759–5769.

(47) Herder, M.; Schmidt, B. M.; Grubert, L.; Pätzelt, M.; Schwarz, J.; Hecht, S. Improving the Fatigue Resistance of Diarylethene Switches. *J. Am. Chem. Soc.* **2015**, *137* (7), 2738–2747.

(48) Sun, W.; Xue, B.; Fan, Q.; Tao, R.; Wang, C.; Wang, X.; Li, Y.; Qin, M.; Wang, W.; Chen, B.; Cao, Y. Molecular Engineering of Metal Coordination Interactions for Strong, Tough, and Fast-Recovery Hydrogels. *Sci. Adv.* **2020**, *6* (16), eaaz9531.

(49) Jing, B. B.; Evans, C. M. Catalyst-Free Dynamic Networks for Recyclable, Self-Healing Solid Polymer Electrolytes. *J. Am. Chem. Soc.* **2019**, *141* (48), 18932–18937.

(50) Burnworth, M.; Tang, L.; Kumpfer, J. R.; Duncan, A. J.; Beyer, F. L.; Fiore, G. L.; Rowan, S. J.; Weder, C. Optically Healable Supramolecular Polymers. *Nature* **2011**, *472* (7343), 334–337.